RSC Advances

PAPER

View Article Online
View Journal | View Issue

Cite this: *RSC Adv.*, 2016, **6**, 105578

Chitosan-folate coated mesoporous silica nanoparticles as a smart and pH-sensitive system for curcumin delivery†‡

Mohammad Porgham Daryasari,[a] Mohammad Reza Akhgar,[a] Fatemeh Mamashli,[b] Bahareh Bigdeli[b] and Mehdi Khoobi*[cd]

In this work, normal and large pore size mesoporous silica nanoparticles (NMSNs and LMSNs) were prepared by co-condensation method and coated with (3-aminopropyl)triethoxysilane (APTES) to prepare amine functionalized MSNs (MSN-NH_2). They were then conjugated with succinic anhydride (SA) to obtain carboxylic acid functionalized MSNs (MSN-COOH). Curcumin (CUR) as a hydrophobic drug was loaded into the synthesized MSNs with two different pore sizes to compare the loading capacity and efficiency. The results showed that LMSNs had 2-fold larger loading efficiency and capacity for CUR than NMSNs. Chitosan (CS), as a pH-sensitive polymer, was also conjugated to folic acid (FA) as an active targeting agent and then coated on the surface of carboxylic acid enriched MSNs *via* electrostatic interaction. The MSNs were fully characterized by scanning electron microscopy (SEM), transmission electron microscopy (TEM), zeta potential analysis, dynamic light scattering (DLS), nitrogen adsorption/desorption analysis, thermo gravimetric analysis (TGA), XRD analysis, NMR and UV-visible spectroscopies. The mechanism of CUR release from CS-FA coated LMSNs was pH-sensitive and *in vitro* release modeling revealed that CUR is released *via* Korsmeyer–Peppas mechanism. No significant toxicity was observed for CUR free MSNs, while the CUR loaded MSNs inhibited proliferation of HeLa and NIH-3T3 cell lines, showing more cytotoxic effect on cancerous HeLa cells. Moreover, the selective cellular uptake of CUR loaded LMSNs-COOH@CS-FA by folate receptor-positive HeLa cells was assessed and confirmed. Hemocompatibility and protein corona of the target carrier were also studied to show negligible hemolytic activity and suitable protein–target LMSNs interactions.

Received 17th September 2016
Accepted 30th October 2016

DOI: 10.1039/c6ra23182a

www.rsc.org/advances

Introduction

Cancer is the second leading cause of death in the world and has a great effect on global health. The global incidence of cancer, and the number of new cancer cases, is continuing to rise.[1] Among the different approaches for cancer treatment, chemotherapeutics agents are still widely used as a practical strategy for the treatment of cancers. Common chemotherapeutic agents are often distinguished by short circulation time, nonspecific cell biodistribution and low delivery efficiency at the targeted tumor tissue which mainly arise from the hydrophobicity and degradability of the administered drug.[2,3]

Nanotechnology has opened a new way to selectively engineer a myriad of different materials and remove all obstacles in front of the conventional formulations. The possibility of engineering nanomaterials with controllable size and morphology as well as programing their surface chemistry with the aid of a multitude of biological and medical functions provide a great opportunity for designed nanoplatforms to reach targeted tissue and selectively destroy cancer cells in the body.[3–5]

However, clinical application of conventional nanocarriers has been still limited due to the premature drug release before reaching to the target, uncontrollable rate of drug release and low local concentration, and inefficient cellular uptake.[6,7]

Among various DDSs, mesoporous silica nanoparticles (MSNs) stand out to be a promising candidate due to some of their conspicuous virtues, such as uniform particle sizes (80–500 nm), large surface areas (>1000 $m^2\ g^{-1}$), high pore volumes (0.5–2.5 $cm^3\ g^{-1}$), tunable pore diameters (1.3–30 nm), and capability of being modified with various functional groups in both exterior and interior surfaces independently. Drug

[a]*Department of Chemistry, Kerman Branch, Islamic Azad University, Kerman, Iran*
[b]*Institute of Biochemistry and Biophysics, University of Tehran, Tehran, Iran*
[c]*Pharmaceutical Sciences Research Center, Tehran University of Medical Sciences, Tehran, Iran*
[d]*Department of Pharmaceutical Biomaterials, Medical Biomaterials Research Center, Faculty of Pharmacy, Tehran University of Medical Sciences, Tehran, Iran. E-mail: m-khoobi@tums.ac.ir; Mehdi.khoobi@gmail.com; Fax: +98-21-66461178; Tel: +98-21-64121113*

† This work is dedicated to the memory of Prof. Abbas Shafiee (1937–2016).

‡ Electronic supplementary information (ESI) available: Scheme S1, Fig. S1–S13 and Tables S1–S4. See DOI: 10.1039/c6ra23182a

encapsulation inside the pores followed by blocking the pore entrances with stimuli responsive agents can endow MSNs with the ability to precise control of release without leaching prior to reaching the targeted cells.

Various polymer coatings were exploited to modify the surface of MSNs and create a more advanced carrier with combined benefits of both components.[8] Compared to the all applied stimulus-sensitive polymer, the pH sensitive polymers as more general and ideal coating agents have been regarded to control selective release of drug at tumor tissue. The pH of tumor environment is lower than normal tissue due to the high rate of glycolysis in cancer cells. This media can act as perfect trigger for selective release of anticancer drugs.[9,10]

Chitosan (CS) is a non-toxic biodegradable polycation with a high number of primary amino groups. These amine functional groups render cationic character to the polymer and are responsible for a range of significant features including *in situ* gelation, mucoadhesion, efflux pump inhibition, high cellular permeability as well as bioavailability for oral administration of drugs which make CS as an outstanding candidate in DDSs. CS can be swelled in cancerous tissues due to their acidic media and this property endows the polymer with the ability of discrimination between normal and cancerous cells for controlled drug release.[11–16]

On the other hand, active targeting can also efficiently increase nanoparticles (NPs) internalization through receptor-mediated endocytosis and improve the efficacy of their payloads.[17–20] This ligand mediated targeting employ the affinity of the ligands on the surface of NPs to increase cellular uptake by the targeted cells receptors that overexpressed in the diseased tissues or cells.[21–26] Folic acid (FA) as an inexpensive, water soluble and stable vitamin without adverse effect on normal cells and low immunogenic response has attracted a great deal of attention for active targeting.[27] The over expression of the FA receptor in epithelial malignancies, such as colorectal, ovarian, and breast cancer cells in comparison with most normal cells make FA conjugates as facile and infallible strategy to promote the receptor-mediated endocytosis of nanoparticles.[28–34] The vesicular trafficking of FA conjugates makes them able to move through many organelles and release efficiently their cargo into the cell cytoplasm.[35]

Curcumin (CUR) as an inexpensive drug and a natural polyphenol compound, is extracted from the herb *Curcuma longa* (turmeric), with a diverse range of therapeutic properties. The anti-proliferative property of CUR as well as its low toxicity, high dose tolerance, and safe profile make it as a suitable candidate for cancer therapy.[36,37] However, the pharmaceutical preparations of CUR are restricted due to its low water solubility and poor bioavailability; the main challenges that can be improved through a proper DDS.[38,39]

So far, a few researches have been performed on the use of modified MSNs for CUR delivery. It has been demonstrated that the amino functionalized MCM-41 as hydrophilic and positively charged particles can comparatively control release of CUR and enhance endocytosis in cancer cells compared to the naked MCM-41.[40] Kotcherlakota *et al.* prepared amino functionalized MSNs with different morphology, particle and pore sizes (KIT-6, MSU-2 and MCM-41) for CUR delivery. It was revealed that the encapsulation efficiency was enhanced by amino functionalized MCM-41 in comparison to other MSNs.[41] In a recent study, Kim *et al.* have developed a CUR delivery system based on MCM-41 with coating layer of tannic acid–Fe(III) complex (MSN-TA), as a pH- and glutathione-responsive DDS. The results showed that CUR loaded MCM-41 induced higher cytotoxicity compared to pure CUR in the presence of MRC5 cells.[42]

In the light of the above mentioned results, in this work, we reported a facile strategy to prepare a pH-sensitive MSNs coated with FA conjugated CS as double responsive targeting DDS. MCM-41 in two different pore sizes was prepared and their CUR loading efficiency (CLE) and CUR loading capacity (CLC) were evaluated. The cytotoxic activity and cellular uptake of MSNs and CUR loaded MSNs were analyzed and compared with CUR in the presence of the folate receptor-positive HeLa cells as cancerous and folate receptor-negative NIH-3T3 cells, as normal cells. Hemolysis assay was also carried out to evaluate biosafety of MSNs on erythrocytes.

Experimental

Materials

Cetyltrimethylammonium bromide (CTAB), tetraethyl orthosilicate (TEOS), (3-aminopropyl)triethoxysilane (APTES), succinic anhydride (SA), *N*-hydroxysuccinimide (NHS), 1-ethyl-3-(3-dimethylaminopropyl)carbodiimide (EDC), ammonium nitrate (NH_4NO_3), folic acid (FA), dimethyl sulfoxide (DMSO) and all other solvents and reagents were purchased from Merck (Darmstadt, Germany) and used without further purification. Curcumin (CUR) was from Merck (Darmstadt, Germany). The HeLa and NIH-3T3 cell lines were purchased from National Cell Bank of Iran (Pasteur Institute, Iran). The cells were incubated in RPMI 1640 (Gibco) media supplemented with 10% heat-inactivated fetal bovine serum (FBS) (Gibco) and 200 μg mL^{-1} streptomycin (Jaberebn-Hayan, Iran) and 500 μg mL^{-1} penicillin (Sigma, USA) at 37 °C in humidified atmosphere and 5% CO_2. Millipore Milli-Q® (Burlington, MA, USA) high purified water was used to make aqueous solutions.

Synthesis of functionalized MSN nanoparticles

Preparation of MSN. NMSNs and LMSNs were prepared according to the reported procedures.[43,44] Briefly, 1.0 g CTAB was added into a solution containing 480 mL of deionized water and 3.5 mL NaOH (2 M). The solution was stirred vigorously at 80 °C for 2 h, and 5 mL TEOS was added to react for another 2 h. The white precipitate was separated by vacuum filtration, washed with ethanol several times and then dried overnight under vacuum at 45 °C to form MSN as a white powder. The same procedure was repeated in the presence of mesitylene as the swelling agent of micelles to prepare LMSN.[45–47] 1.0 g of CTAB and 7.0 mL of mesitylene were added to a solution containing 480 mL of deionized water and 3.5 mL of NaOH (2 M). After vigorous stirring at 80 °C for 4 h, 5.0 mL of TEOS was rapidly added into the solution. The reaction was vigorously stirred at 80 °C for

another 2 h. The prepared white precipitate was collected as mentioned above.

Preparation of MSN-NH_2. 1.0 g of MSN was dispersed in 100 mL of deionized water, and then 1 mL of APTES was added into the solution and stirred for 36 h at room temperature. The reaction mixture was then heated for 2 h at 80 °C to prepare amino functionalized MSN. The resulting solution was washed several times with ethanol followed by centrifugation and finally dried overnight under vacuum at 45 °C to achieve MSN-NH_2 as white precipitate.[46]

Preparation of MSN-COOH. SA was employed for surface carboxylation of the MSNs.[46] Briefly, 0.5 g of MSNs-NH_2 were dispersed in 10 mL of anhydrous DMF and sonicated for 10 min to homogenize the suspension. 3 g of SA was dispersed in 10 mL of anhydrous DMF and added to the suspension of MSNs-NH_2. The reaction mixture was stirred over night at room temperature. Finally, the MSNs-COOH were washed with ethanol for several times and dried overnight under vacuum at 45 °C.

CTAB was removed using ionic exchange method.[48] In summary, 1 g of prepared MSNs were dispersed in 100 mL of ethanol (95%) containing 1 g of NH_4NO_3, and refluxed for 6 h at 80 °C. The removed template MSNs were recovered by filtration; washed with ethanol and dried overnight under vacuum at 45 °C. To improve the efficiency of the process, the above procedure was repeated for two times.

Conjugation of FA to CS. Conjugation of FA to CS was done according to the following method.[31,35] A solution of FA (0.56 g) and EDC (0.2 g) in anhydrous DMSO (20 mL) was prepared and stirred at room temperature until EDC and FA were well dissolved (2 h). The solution was then added dropwise to the solution of CS 0.5% (w/v) in acetate buffer (0.1 M, pH 4.7). The obtained mixture was stirred at room temperature in dark for 16 h to accomplish conjugation of FA to CS and then the pH was adjusted to 9.0 by addition of NaOH (1.0 M). Thereafter, the resulting yellow precipitate was collected by centrifugation at 2500 rpm (Hettich, ROTINA 380R, Rotor with max. rate of 1000 rpm, Germany). The precipitate was dialyzed first against phosphate buffered saline (PBS, pH 7.4) for 3 days and then against water for 4 days. At the final step, the FA conjugated CS was isolated by lyophilization.

Preparation of CS-FA coated MSNs. CS-FA coated LMSNs were prepared according to the reported procedure with some modifications:[49] 25 mg CS-FA powder was dispersed in 5 mL (3%) acetic acid and then the mixture was stirred for 24 h to prepare a solution of CS-FA (0.5% w/v). 10 mg of LMSNs were dispersed in 5 mL ethanol for 10 min, and the pH was adjusted to 3.5–4.5 by addition of acetic acid. Subsequently, 5 mL of the CS-FA solution (0.5%) was added into the mixture and allowed to stir at room temperature for 24 h. The CS-FA coated MSNs were collected by centrifugation at 10 000 rpm to separate the yellow precipitate from solution which was washed with deionized water and excess ethanol before freeze drying.

Ninhydrin assay

Determination of primary amines content on the amino modified samples was carried out by ninhydrin colorimetric assay.[50,51] Briefly, 1 mL color reagent (10 g of $Na_2HPO_4 \cdot 12H_2O$, 6 g of KH_2PO_4, 0.5 g of ninhydrin in 100 mL of distilled water) was added into a dispersed solution of 3 mg of sample in 2 mL of distilled water, and the mixture was heated in the boiling water bath for 16 min and then cooled in the water bath at 20 °C for 20 min. Afterward 5 mL of diluting solution (2 g of KIO_3 in 600 mL distilled water and 400 mL of ethanol 96%) was added to the mixture. The color of the solution turns to purple blue due to the reaction of the amino groups with ninhydrin. The yield of the reaction was measured by UV-visible spectrophotometer at 570 nm. The reaction of APTES with ninhydrin was applied for preparation of the calibration curve.

Loading of CUR in MSNs

CUR was loaded into the MSN-COOH according to the reported method with some modifications.[52] 30 mg of dry MSN-COOH was added in 5 mL of CUR solution in dichloromethane (1 mg mL^{-1}), and the mixture was sonicated for 5 min by ultrasonic bath to obtain a well dispersed suspension. After stirring for 48 h under light sealed conditions, the CUR loaded MSNs were collected by centrifugation and washed with deionized water. To calculate the CUR loading efficiency (CLE) and loading capacity (CLC), the residual CUR content in the supernatant was determined through plotting calibration curve of CUR standard solutions by UV-visible measurement at 420 nm. The CUR loading efficiency and capacity were calculated as follows:

$$\text{CLE (\%)} = \text{mass of loaded CUR in MSN/total mass of CUR added initially} \times 100$$

$$\text{CLC (\%)} = \text{mass of loaded CUR in MSN/mass of MSN} \times 100.$$

In vitro CUR release profile

The release profile of CUR was investigated as follow: Tween-80 0.1% (w/v) was added to the phosphate buffer saline (PBS) to facilitate the release and dissolution of CUR in aqueous phase and maintain a sink condition. 2 mg of the sample was immersed into the 3 mL PBS (pH 7.4 with 0.1% Tween-80) and (pH 5.5 with 0.1% Tween 80) tubes. The release assay was performed at 37 °C in dark using a shaking water bath at 100 rpm. Sampling was done at predetermined time points. In each time point, all release medium was taken out by centrifugation at 10 000 rpm for 15 minutes and replaced with equivalent volume of fresh medium. The cumulative release profile of CUR was evaluated by UV-visible spectrophotometry (at 420 nm). The calibration curve of the released CUR concentration was plotted by given concentration of CUR standard solutions in the same condition.[52,53] *In vitro* release kinetics modeling was analyzed by KinetDS 3 rev 2010 software.

Cellular uptake analysis

Flow cytometric analysis was investigated for cellular uptake of CUR loaded MSNs. Owing to the intrinsic green fluorescence of CUR, cellular uptake of CUR and CUR-loaded MSNs was studied by flow cytometry. NIH-3T3 and HeLa cells were grown in 6-well

plates (40 000 cells per well) up to 80% confluency. Cells were then treated with freshly prepared serum-free medium (pH 6) containing 100 μg mL^{-1} of CUR (in the form of free CUR or CUR loaded MSN-COOH, LMSN-COOH@CS or LMSN-COOH@CS-FA). After 30 min incubation, the cells were trypsinized, washed with PBS three times, and resuspended in 1 mL PBS.[54] CyFlow Space (Parpec, Germany) flow cytometer was used to examine cellular uptake and FloMax software was used to analyze the data.

MTT cell viability assay

Cytotoxicity of the drug loaded MSNs was determined by MTT (3-(4,5-dimethyl thiazol-2-yl)-2,5-diphenyl tetrazolium bromide) assay against NIH-3T3 fibroblasts and HeLa cells as normal and tumor cells, respectively. NIH-3T3 and HeLa cells were separately seeded in 96-well plates at the density of 7×10^3 cells per well and culture medium of RPMI (200 μL). After 24 h incubation to allow cells to attach, the media were replaced with fresh media containing LMSN-COOH, LMSN-COOH@CS-FA, LMSN-COOH-CUR@CS-FA (prepared in deionized water), and CUR (prepared in DMSO with safety concentration of 0.1%) at a concentration range of 0.1–100 μg mL^{-1} and in a total volume of 200 μL. The plates were then further incubated at 37 °C for 72 h. 100 μL of PBS containing 5 mg mL^{-1} MTT (Sigma, USA) was then added to each well. After cells incubation for an additional 4 h, 100 μL of DMSO was added to each well. The absorbance of each well was read on Bio Tek microplate reader (USA) at a test wavelength of 570 nm and a reference wavelength of 630 nm. Cell viability was calculated based on the following formula:[55]

$$\text{Number of viable cells} = (\text{Abs of sample} \times 100)/(\text{Abs of control}).$$

Hemolysis assay

For hemolysis assay, the human red blood cells (HRBCs) were obtained according to the reported procedure.[37,56] Briefly, the fresh human blood was stabilized and treated with EDTA to remove the plasma as supernatant by centrifugation at 2000 rpm for 10 min and refined by successive rinsing with PBS buffer (pH 7.4). The suspension of HRBCs was diluted 10 times with PBS buffer (pH 7.4), and then 200 μL of HRBCs suspension was added to 800 μL of each sample with different concentration (1.95–1000 μg mL^{-1}). In the case of positive control, 200 μL of HRBCs suspension was added to 800 μL Triton X_{100} (2% v/v), and for negative control 200 μL of HRBCs suspension was added to 800 μL of PBS buffer (pH 7.4). Afterwards, all of the samples were incubated for 2 h at room temperature by moderate shaking. Finally, the samples were centrifuged at 10 000 rpm for 2 min, and the absorbance of supernatant (hemoglobin) was measured by UV-visible spectrophotometer at 541 nm. The hemolytic activity percentages of the different samples were calculated as follows:

$$\text{Hemolysis}\% = (\text{Abs}_{\text{sample}} - \text{Abs}_{\text{ctrl}}{}^{-}/\text{Abs}_{\text{ctrl}}{}^{+} - \text{Abs}_{\text{ctrl}}{}^{-}) \times 100.$$

Preparation of protein corona

The protein coated MSNs were prepared by incubating the MSNs with plasma proteins at protein concentrations of 10% (simulation of an *in vitro* milieu) and 100% (simulation of an *in vivo* milieu) for 1 h under slow stirring at 37 °C (human body temperature) to allow proteins to condense onto the surface of MSNs. Plasma proteins coated MSNs (at concentration of 10%) were prepared by adding 100 μL of MSNs (1 mg mL^{-1}) to stock solution of 100 μL plasma protein in 800 μL PBS (pH = 7.4), and the above sample at the concentration of 100% was prepared by adding 100 μL of MSNs (1 mg mL^{-1}) to stock solution of 900 μL plasma protein to confirm complete surface coverage. After incubation, samples were centrifuged for 3 times at the following conditions: (1) at 11 000 rpm for 30 min where the supernatant was removed and replaced with 500 μL PBS, (2) and (3) at the same condition of the first step while the samples were centrifuged for 20 min. Washing steps were performed to remove the loosely attached proteins from the surface of the MSNs and leave only the strongly bound "hard corona" proteins attached to the MSNs.[57–59] Separation of protein samples was done by SDS-PAGE to investigate hard corona protein. For this purpose, 50 μL of each sample was mixed with 15 μL of sample buffer [Tris-base, pH 6.8, SDS 10% (w/v), bromophenol blue (10% w/v), glycerol (20% w/v), 2-mercaptoethanol (10% w/v)] and immersed in water bath at 100 °C for 15 min. Equal volumes of the samples were loaded on 12% acrylamide SDS-PAGE, run for 4 h at 120 V, 20–30 A. Silver nitrate staining method was used to demonstrate proteins in gel. Gel densitometry was analyzed by Gel Analyzer 2010 software.

Characterization

In order to verify the successful functionalization of MSNs, Fourier transform infrared spectroscopy (FTIR) were taken by FT-IR Magna 550, Nicolet using the KBr plates. NMR experiment was recorded on Avance III ultrasheild spectrometer manufactured by Bruker at a field strength of 11.7 tesla (500 MHz) and spectroscopy data are collected using TopSpin software. Powder XRD patterns were collected on STOE Theta–theta Powder Diffraction System, radiation: 1.54060 Cu, generator: 40 kV, 40 mA. Surface area analyzer (Quantachrome NOVA Automated Gas Sorption System, 2000e) was used to calculate nitrogen adsorption isotherm, specific surface area (by BET method) and pore size distribution curve (by BJH method). Thermal decomposition experiments were carried out by thermogravimetric analysis (TGA) on Thermogravimetric analyzer METTLER TOLEDO from room temperature to 800 °C under nitrogen flow. UV-visible spectra measurements were acquired using UV-visible Jasco-530 spectrophotometer in the range of 220–800 nm. Hydrodynamic size distribution and zeta potential were determined by using a ZEN3600 Zetasizer (Malvern Instruments, UK). The morphology of the samples was investigated by transmission electron microscope (HRTEM, Philips CM30, 300 kV, Netherlands) and field emission scanning electron microscope (FE-SEM, Tescan/Mira, Czech Republic).

Results and discussion

This study mainly focused on the preparation of active and passive targeted MSNs, and investigation of the effect of pore

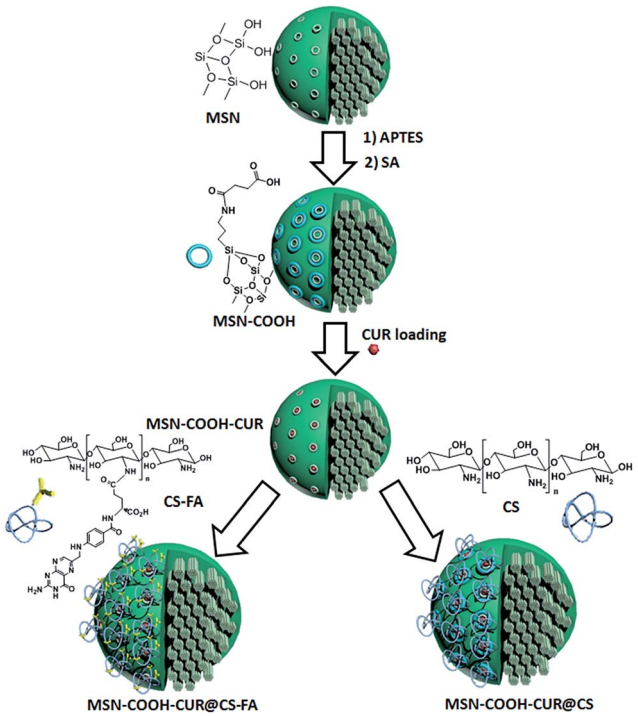

Scheme 1 MSNs functionalization and CUR loading.

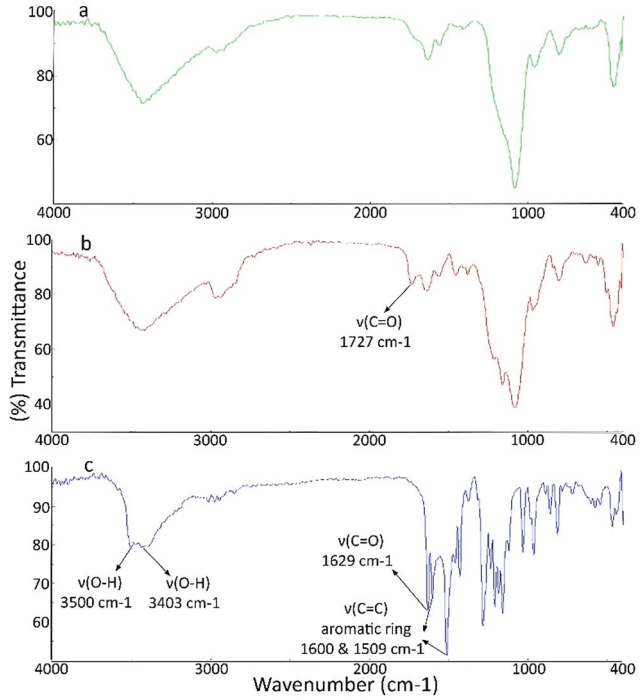

Fig. 1 FT-IR spectra of LMSN-COOH@CS-FA (a), LMSN-COOH-CUR@CS-FA (b) and CUR (c).

size on the loading efficiency and surface coating on the mechanism of the drug release, and biocompatibility. Scheme 1 shows the sequence steps for the preparation of the target MSNs and drug loading. MSNs were prepared and functionalized with APTES followed by SA to obtain carboxylic acid functionalized MSN-COOH. CUR was then loaded into the pores of MSNs after template removing using ionic exchange method. CUR loading efficiency and capacity were assessed for both LMSNs and NMSNs. Since the best results were achieved for LMSNs, the next modification was done for LMSNs. CS was conjugated with FA and then coated on the surface of LMSNs *via* electrostatic interaction to provide an active and passive targeted CUR delivery system. All samples were fully characterized and evaluated in the viewpoint of their cytotoxicity, blood compatibility, and plasma proteins interaction as well as CUR release at different pH.

Characterization of MSNs

FT-IR analysis. The FT-IR spectra of LMSN-COOH@CS-FA, LMSN-COOH-CUR@CS-FA and CUR are shown in Fig. 1. The FT-IR spectra of LMSN and all functionalized LMSNs showed absorption peaks of silanol groups at around 1090 cm^{-1}, 800 cm^{-1}, and 470 cm^{-1} which are attributed to Si–O bonds (Fig. S2, see ESI‡). In the spectrum of LMSNs, the absorption peak at around 2900 cm^{-1} is attributed to C–H stretching vibrations (ν_{CH}) which disappeared in the LMSN after the template is removed (Fig. S2, see ESI‡). The appeared band in the spectrum of LMSN-NH_2 at around 1645 cm^{-1} could be ascribed to the bending vibration (δ_{N-H}) of N–H bond. The new appeared band at around 1725 cm^{-1} in the spectrum of LMSN-COOH could be attributed to the C=O stretching vibrations ($\nu_{C=O}$) of the new carboxyl acid groups. Also, the intensity of the band at around 1640 cm^{-1} was obviously increased which may be assigned to the stretching vibrations of amide bonds (Fig. S2, see ESI‡). The FTIR spectrum of CUR exhibited a sharp peak at 3490 cm^{-1} and a broad peak at about 3400 cm^{-1} relating to the OH groups of CUR. The bands appeared at around 1629 and 1600 cm^{-1} are attributed to the stretching vibration of C=O bonds and C=C aromatic rings. All other bands were in agreement with the FT-IR spectrum of CUR. The FT-IR spectrum of the CUR loaded MSNs showed the combined characteristic peaks of CUR and MSNs (Fig. 1).

NMR analysis. The successful conjugation of CS with FA was confirmed by ^{1}H NMR spectroscopy. The presence of signals at δ 1.65, 2.88, and 3.08–3.64 ppm could be attributed to the protons resonance of the $-COCH_3$, –CH–NH–, and $-CH_2-O-$ groups in CS, respectively. The protons resonance of folate moiety in CS-FA conjugate was also observed at δ 6.3–8.5 ppm (Fig. S3‡).[31,35]

Morphological analysis of MSNs. As shown in Fig. 2, all MSNs were in spherical shape and proper size distribution. Fig. 2b and d are related to the presence of CS-FA layer on the surface of MSNs. As shown in the TEM images (Fig. 2c) highly ordered mesoporous network with a hexagonal array and classified pores could be clearly seen in the pure MSN nanoparticles. The CS-FA shell around the core of nanoparticles could be seen in Fig. 2d.

Zeta potential analysis and dynamic light scattering (DLS). Surface zeta potential gives an evidence for the potential stability of nanoparticles colloidal system and can be

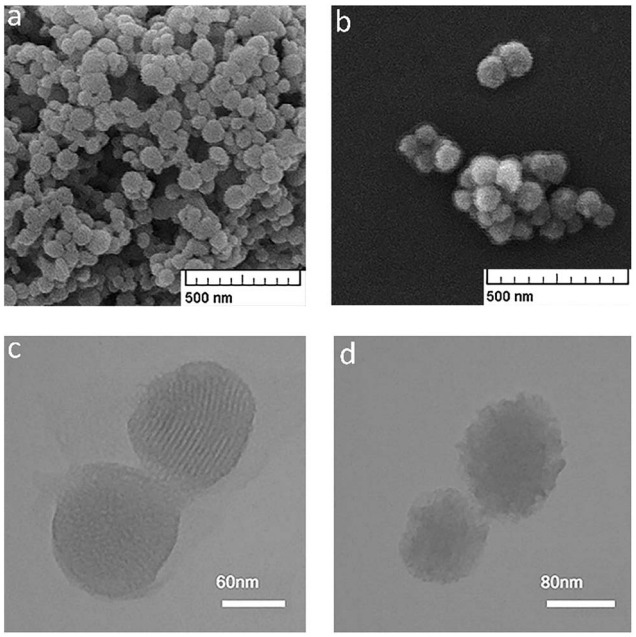

Fig. 2 Morphological characterization of MSNs: FE-SEM images of LMSNs-removed (a), LMSN-COOH@CS-FA (b); TEM image of LMSNs-removed (c) and LMSN-COOH@CS-FA (d).

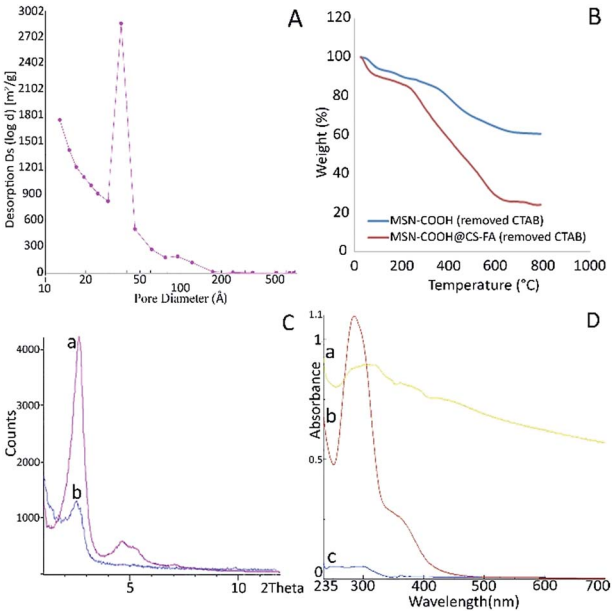

Fig. 3 BJH pattern of LMSN-removed (A); TGA curves of LMSN-COOH and LMSN-COOH@CS-FA (B); XRD pattern of (a) LMSN and (b) LMSN-COOH@CS-FA after the removal of template (C) and UV-visible spectrum of (a) FA, (b) CS-FA and (c) CS (D).

considered as an important measurement to explicate their mutual interactions. If all the particles in suspension have a high negative or positive zeta potential value, they will tend to repel each other resulting in no affinity to aggregate and weak mutual interactions.[60] The results showed an obvious increase in zeta potential of naked LMSNs from −19.8 mV to +51 and +20 mV in LMSN-NH_2 and LMSN-COOH, respectively. In the case of LMSN-COOH@CS and LMSN-COOH@CS-FA the results showed decrease in zeta potential from +38.6 to +20.4, respectively. This might be due to modification of CS coating layer by FA and consequently, causing a reduction in the amount of protonated amino group and a drop of zeta potential.[61,62] These charge alterations confirmed properly surface functionalization of LMSNs. Particle size distribution of MSNs was determined by DLS to provide hydrodynamic diameter of the LMSNs. The CS-FA coating layer increased the overall particle size comparing to LMSNs without coating layer. The results were in a good agreement with the obtained results by FE-SEM/TEM images of MSNs (Fig. S4 and Table S1, see ESI‡). However, differences in NPs size between DLS and FE-SEM/TEM measurements can be attributed to the hydrodynamic radius and water swollen NPs for DLS measurement; whereas TEM/SEM represented an estimation of NPs diameter in dried state.[37]

N_2 adsorption and desorption analysis. The specific surface areas were calculated by the Brunauer–Emmett–Teller (BET) method[63,64] and pore size diameters were obtained from the desorption branches of the isotherms by BJH methods (Fig. 3A and S5‡).[65] N_2 adsorption and desorption isotherms of the NMSN, CTAB removed NMSN and LMSN exhibited a type IV isotherm corresponding to a cylindrical mesoscale pore structure. The sharp increase at a relative pressure of 0.2–0.8 (P/P_0) could be related to the capillary condensation of N_2 and narrow pore size distribution or uniform pore sizes, (Table S2 and Fig. S6, see ESI‡). The results showed that using swelling agent in the synthesis of LMSN increased the pore sizes as well as surface area ($S = 1096.05$ m^2 g^{-1} and $d = 36.37$ Å).

Thermo gravimetric analysis (TGA). TGA analysis under a constant N_2 flow was performed to gain some structural information about the surface modified MSNs. Fig. 3B shows the TGA of LMSN-COOH and LMSN-COOH@CS-FA. The first step of weight loss in thermogram of both MSNs can be seen over the range of about 25–300 °C indicating the evaporation of residual solvent and adsorbed water. Weight loss of about 28% in second step, at the range of 300–650 °C could be attributed to the removal of organic moiety on the surface of LMSN-COOH nanoparticles. Comparison between these thermograms indicated that a weight loss of about 35% at the range of 300–650 °C could be ascribed to removal of CS-FA coating layer on the surface of LMSN-COOH@CS-FA.

XRD analysis. The obtained XRD patterns of the LMSN and LMSN-COOH@CS-FA after the removal of the template confirmed the formation of the hexagonal structure of LMSNs and confirmed preserving of the crystalline structure of LMSNs after surface modification (Fig. 3C). The XRD pattern of LMSN-COOH@CS-FA showed a slight decrease in the intensity in comparison with LMSN which could be due to the presence of CS-FA on the surface of LMSNs. These results are in accordance with the recently published reports.[16,51]

Ninhydrin and UV-visible analyses. The absorbance of the ninhydrin complex with primary amine at 570 nm could be utilized to calculate the amine density (Fig. S7, see ESI‡). The amino contents of the samples were listed in Table S3.‡ The results showed that 36.61% of amino groups on the surface of

LMSN-NH_2 were converted to acid groups after reaction with SA. Also, the amount of FA conjugation with CS was 24.48%. UV-visible spectra of CS before and after conjugation with FA and the appeared peak at around 300 nm were also used to confirm formation of CS-FA conjugate (Fig. 3D).[36]

CUR loading into MSNs. The drug loading in MSNs is influenced by the pore size.[66] CUR loading efficiency (CLE) and CUR loading capacity (CLC) as two important parameters to investigate the capability of a carrier was calculated by UV-visible spectrophotometer (Fig. S8 and S9, see ESI‡). The results showed that CLE and CLC were 31.2% and 4.6% for LMSN-COOH respectively; while NMSN-COOH showed a lower CLE of 15.7% and CLC of 2.7%. It could be concluded that the decrease in the pore size of MSNs led to a drop in CLE and CLC.

***In vitro* CUR release profile.** Fig. 4 depicts the profiles of CUR release from different types of CUR loaded MSNs in two different pH values of 7.4 and 5.5 representing biological environment (bloodstream) and endocytic compartments, respectively.[67] As seen, there was a pH-sensitive behavior for CUR release from LMSN-COOH-CUR@CS-FA, so that about 49%, 63%, and 70% of CUR was released from CS-FA coated MSNs at 24, 72, and 96 h, respectively, which was 2.33-fold (at 24 h), 2.25-fold (at 72 h), and 2.12-fold (at 96 h) larger than that at pH 7.4. Considering the slight, ignorable difference in CUR release from LMSN-COOH-CUR at pH 5.5 and 7.4, we concluded that the presence of CS-FA coating layer on the surface of MSNs could be the main reason to explain the pH-sensitive CUR release from LMSN-COOH-CUR@CS-FA.[68] It could be attributed to the high permeability and swelling ability of CS at acidic environments.[10,69] From another point of view, a comparison between the profiles of CUR release from LMSN-COOH-CUR and LMSN-COOH-CUR@CS-FA at pH 5.5 indicates the sustained CUR release from LMSN-COOH-CUR@CS-FA, as the CUR released from LMSN-COOH-CUR promptly reached a plateau within 6 h (equal to 80% accumulated CUR release); whereas, the accumulated amount of CUR release from LMSN-COOH-CUR@CS-FA was only 24% at the same time and gradually reached 70% after 96 h. Furthermore, the accumulated amount of CUR release from LMSN-COOH-CUR was averagely 10 percent more than that for NMSN-COOH-CUR at pH 5.5 and 7.4 which might be related to the difference in pore size of LMSNs and NMSNs.[66]

In sum, the prepared DDS demonstrated a pH-sensitive and sustained CUR release behavior which is of crucial importance for selective and efficient treatment of diverse types of cancers. For further studies, the *in vitro* release modeling was performed to predict the release profile kinetics by most used mathematical models, zero-order, first-order and Korsmeyer–Peppas.[70] The results were listed in Table S4.‡ In order to fit of a model equation, best mathematical model was chosen by using the coefficient of determination (R^2). According to the R^2 results, release data were found to be adjusted to Korsmeyer–Peppas model. This model is generally used to evaluate the release profile mechanism particularly when more than one parameter or not well known mechanism involved.[71] In order to determine release mechanism, n value in Korsmeyer–Peppas model, consist of $n \leq 0.45$ for Fick diffusion mechanism and $0.45 < n \leq 1.0$ for mass transfer following non-Fickian or anomalous diffusion model were determined.[70,71]

As mentioned above, CUR release from LMSN-COOH-CUR@CS-FA at pH 5.5 and 7.4 seems to be controlled by non-Fickian diffusion. In non-Fickian diffusion mechanism, the kinetic of CUR release is controlled by both diffusion and polymer swelling, while the release kinetic of LMSN-COOH-CUR and NMSN-COOH-CUR at pH 5.5 and 7.4 seems to be described by Fickian diffusion and system acts as a simple barrier.[72] In sum, good correlation could be observed between experimental and linear regression data.

Cellular uptake studies. Fig. 5 and S10‡ depicts the histograms of cellular CUR fluorescence in HeLa and NIH-3T3 cells incubated with CUR, LMSN-COOH-CUR, LMSN-COOH-CUR@CS, and LMSN-COOH-CUR@CS-FA. The untreated cells, as negative control, were used to measure autofluorescence. Based on the obtained results, free CUR appeared to be more effective in penetrating both cell lines than CUR loaded MSNs. This could be due to the hydrophobic nature of CUR as a small molecule material which can easily diffuse through

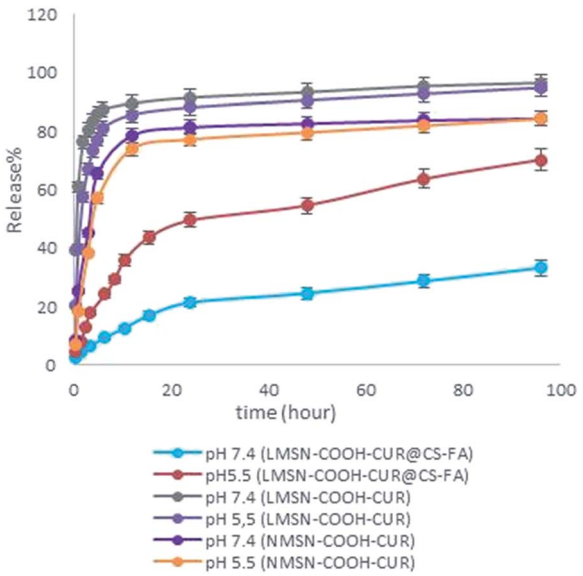

Fig. 4 Release profiles of CUR from LMSNs and NMSNs.

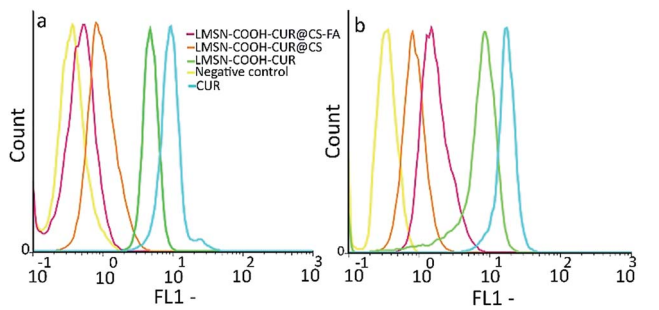

Fig. 5 Flow cytometric analysis of CUR, LMSN-COOH-CUR, LMSN-COOH-CUR@CS, and LMSN-COOH-CUR@CS-FA cellular uptake in (a) NIH-3T3 and (b) HeLa cells.

phospholipid cell membrane.[73] Furthermore, cell internalization of CUR in HeLa cells was almost 2-fold higher than that in NIH-3T3 cells which could be attributed to the fact that the different internal hydrophobic environment of tumor cells and normal cells leads to diverse CUR–cell interactions.[74] For CS and CS-FA coated MSNs, cellular uptake of LMSN-COOH-CUR@CS in NIH-3T3 was about 1.5-fold greater than that of LMSN-COOH-CUR@CS-FA which could be related to the more positive charge density of CS in comparison to CS-FA (see Tables S1 and S3‡). Therefore, the interaction of positively charged MSNs with the negatively charged cell membrane (adsorptive-mediated endocytosis) can be the most probable mechanism of the cellular uptake in this case.[75] On the other hand, cellular uptake of LMSN-COOH-CUR@CS-FA in HeLa cells was about 2-fold greater than that of LMSN-COOH-CUR@CS, mainly owing to the interaction of FA with overexpressed folate receptors on the surface of HeLa cells which results in selective cell internalization of LMSN-COOH-CUR@CS-FA *via* the mechanism of receptor-mediated endocytosis.[76] Moreover, the 3-fold higher cell internalization of LMSN-COOH-CUR@CS-FA in HeLa cells, in comparison with folate receptor-negative NIH-3T3 cells, can be another evidence to support this hypothesis. Since almost 25% of CUR releases from MSN-COOH-CUR at 30 min at pH 6, the cellular uptake of MSN-COOH-CUR might be a combination of free CUR cell penetration *via* free diffusion and MSN-COOH-CUR cell internalization through adsorptive-mediated endocytosis.

MTT assay. Fig. 6 and S11–S14‡ demonstrate the cytotoxicity of CUR free MSNs, CUR loaded MSNs, and CUR against NIH-3T3 and HeLa cell lines after 24, 48, and 72 h of incubation. As exhibited in Fig. S11 and S12,‡ LMSN-COOH, LMSN-COOH@CS, and LMSN-COOH@CS-FA showed almost no cytotoxic effect on both cell lines revealing their biocompatible property (about 95% cell viability at high concentration after 72 h). On the other hand, CUR loaded MSNs including LMSN-COOH-CUR, LMSN-COOH-CUR@CS, and LMSN-COOH-CUR@CS-FA demonstrated a diverse behavior for both cell lines (Fig. 6 and S13, S14‡). For NIH-3T3 cells, cytotoxicity of LMSN-COOH-CUR@CS was relatively more than that of LMSN-COOH-CUR@CS-FA (about 3% at top concentration) which could be probably due to the higher cellular uptake of LMSN-COOH-CUR@CS leading to more CUR accumulation in cytoplasm (Fig. 5). But for HeLa cells, noticeably higher cytotoxicity activity for LMSN-COOH-CUR@CS-FA was obtained (averagely 17% at top concentration) than LMSN-COOH-CUR@CS.

In comparison, LMSN-COOH-CUR exhibited significantly cytotoxicity as compared to CS and CS-FA coated MSNs which could be related to the high CUR release from LMSN-COOH-CUR (Fig. 4). In fact, the absence of CS and CS-FA coatings leads to prompt CUR release from MSNs and therefore more free diffusion of free CUR through phospholipid cell membrane (Fig. 6 and S13, S14‡).[67,77] Moreover, slow and sustained CUR release from CS and CS-FA coated MSNs could be another reason for low cytotoxicity of LMSN-COOH-CUR@CS and LMSN-COOH-CUR@CS-FA in both cell lines as compared to free CUR.[77,78]

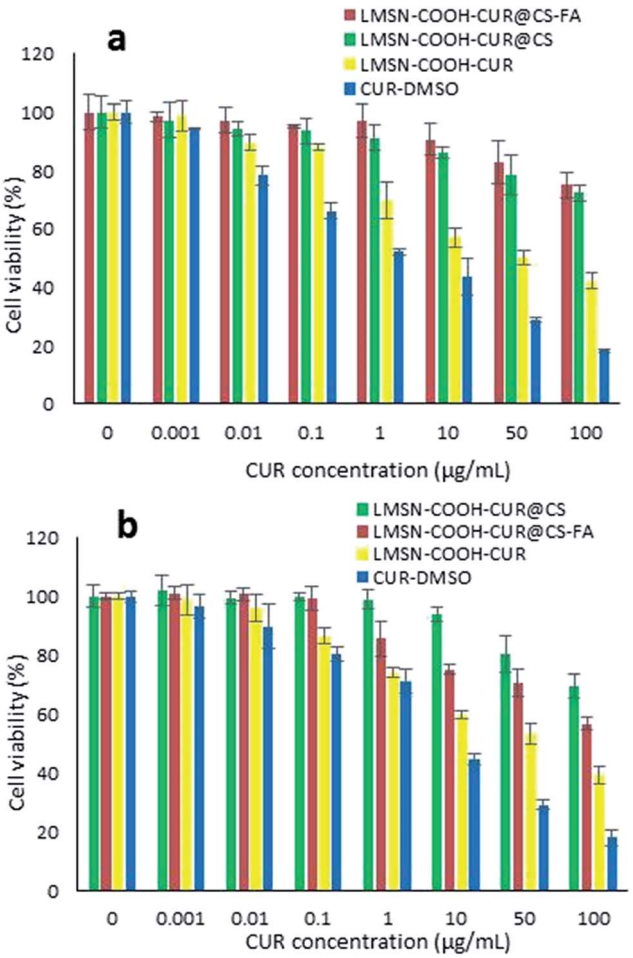

Fig. 6 Cytotoxicity of free and CUR loaded nanoparticles measured by MTT assay in NIH-3T3 (a) and HeLa (b) cells after 72 h incubation. Data is expressed as mean ± S.D. ($n = 3$).

Hemolysis assay. Hemocompatibility of MSNs can be confirmed by *in vitro* cytotoxicity assay to evaluate biosafety of MSNs on erythrocytes.[37,56] As depicted in Fig. 7, LMSN-COOH-CUR@CS-FA showed good hemocompatibility, similar to the PBS (negative control). In comparison, the HRBCs treated with Triton X_{100} (2% v/v) (positive control) displayed obvious hemolysis activities. As shown in Fig. 7a and b, the percentages of hemolytic activity for both MSNs in the studied concentration range (1.95–1000 μg mL^{-1}) were less than 5% (standard acceptance limit), suggesting their exceptional hemocompatibility. The maximum hemolytic activity percentage of LMSN-COOH-CUR@CS-FA was 1.75%.

Protein corona study. Surface of nanoparticles become covered with a condensed layer of plasma protein quickly after entering in the body and change their destiny before reaching to the intended target.[53,79] The inclination of protein to coating nanoparticles may depend on particle size and surface properties of the nanoparticles. In this study, the effect of CS-FA coating layers on the protein corona formation in two condition protein concentrations of 10% (simulation of an *in vitro* milieu) and 100% (simulation of an *in vivo* milieu) was

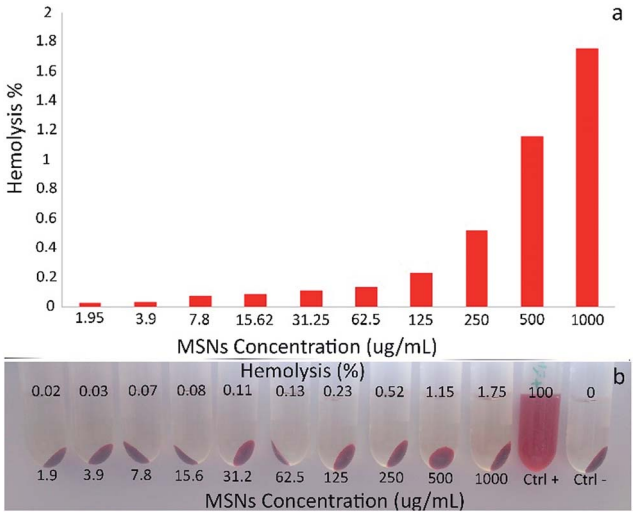

Fig. 7 Hemolytic activity and hemolysis percentage of LMSN-COOH-CUR@CS-FA (a), Photographs of RBCs treated with LMSN-COOH-CUR@CS-FA at different concentrations (b).

investigated by SDS gel electrophoresis. It has been revealed that surface functional groups of the nanoparticles as well as protein concentrations can control protein corona.[57,79] As shown in Fig. S15,‡ all LMSNs in 10% plasma protein concentration were enriched by the protein with <45 kDa molecular weight. Increasing of the protein corona for LMSNs coated with CS-FA could be due to the positive surface charge of CS-FA layer. The intensive protein band could be observed in the range of 45–75 kDa and >75 kDa for LMSNs in 100% plasma protein concentration which could be due to the increased interaction between the CS-FA layers and more plasma proteins.

Conclusion

There has been a considerable interest to design and develop passive and active targeting DDSs with a novel approach focused on enhancing aqueous solubility of hydrophobic drugs and improving the drug loading capacity, therapeutic efficacy, and sustained release. To achieve this goal, herein we introduced LMSNs coated with FA conjugated CS as a smart nanocarrier for targeted delivery of CUR as model hydrophobic anticancer drug. The results showed an increase in loading capacity, pH dependent and sustained *in vitro* release profile, and biocompatibility. Our findings exhibited that CUR free LMSNs were safe for normal cell lines, and folate receptor-positive HeLa cell line was more sensitive to the anti-proliferative effect of CUR as a result of higher cellular uptake of CS-FA coated LMSNs by HeLa cells than folate receptor-negative NIH-3T3 cell line. These results confirmed selective targeting and successful delivery of CUR by the designed MSNs. These findings suggest LMSN-COOH-CUR@CS-FA as a promising candidate for targeted hydrophobic anticancer delivery. Study on biodistribution of the carrier and its tumor shrinking power *via in vivo* analyses could be the objects of future researches.

Acknowledgements

This study was supported by a grant from the Research Council of Tehran University of Medical Sciences (Grant no. 30429) and from the Iran National Science Foundation (INSF; Grant no. 92037263).

References

1 A. Jemal, R. Siegel, E. Ward, Y. Hao, J. Xu and M. J. Thun, *Ca-Cancer J. Clin.*, 2009, **59**, 225–249.
2 K.-N. Yang, C.-Q. Zhang, W. Wang, P. C. Wang, J.-P. Zhou and X.-J. Liang, *Cancer Biol. Med.*, 2014, **11**, 34–43.
3 N. T. Phuoc, J. F. Quinn, M. R. Whittaker and T. P. Davis, *Polym. Chem.*, 2016, **7**, 4295–4312.
4 S. Wilhelm, A. J. Tavares, Q. Dai, S. Ohta, J. Audet, H. F. Dvorak and W. C. Chan, *Nature Reviews Materials*, 2016, **1**, 16014.
5 N. T. Tran, Z. Jia, N. P. Truong, M. A. Cooper and M. J. Monteiro, *Biomacromolecules*, 2013, **14**, 3463–3471.
6 M. Talelli, M. Iman, A. K. Varkouhi, C. J. Rijcken, R. M. Schiffelers, T. Etrych, K. Ulbrich, C. F. van Nostrum, T. Lammers and G. Storm, *Biomaterials*, 2010, **31**, 7797–7804.
7 S. Mura, J. Nicolas and P. Couvreur, *Nat. Mater.*, 2013, **12**, 991–1003.
8 S. B. Hartono, N. T. Phuoc, M. Yu, Z. Jia, M. J. Monteiro, S. Qiao and C. Yu, *J. Mater. Chem. B*, 2014, **2**, 718–726.
9 M. Stubbs, P. M. McSheehy, J. R. Griffiths and C. L. Bashford, *Mol. Med. Today*, 2000, **6**, 15–19.
10 J. Liu, Y. Huang, A. Kumar, A. Tan, S. Jin, A. Mozhi and X.-J. Liang, *Biotechnol. Adv.*, 2014, **32**, 693–710.
11 P. C. Berscht, B. Nies, A. Liebendörfer and J. Kreuter, *Biomaterials*, 1994, **15**, 593–600.
12 M. Thanou, J. Verhoef and H. Junginger, *Adv. Drug Delivery Rev.*, 2001, **50**, S91–S101.
13 M. Thanou, J. Verhoef and H. Junginger, *Adv. Drug Delivery Rev.*, 2001, **52**, 117–126.
14 S. A. Agnihotri, N. N. Mallikarjuna and T. M. Aminabhavi, *J. Controlled Release*, 2004, **100**, 5–28.
15 X. Qu, A. Wirsén and A. C. Albertsson, *J. Appl. Polym. Sci.*, 1999, **74**, 3186–3192.
16 A. Popat, J. Liu, G. Q. M. Lu and S. Z. Qiao, *J. Mater. Chem.*, 2012, **22**, 11173–11178.
17 J. Hrkach, D. Von Hoff, M. M. Ali, E. Andrianova, J. Auer, T. Campbell, D. De Witt, M. Figa, M. Figueiredo and A. Horhota, *Sci. Transl. Med.*, 2012, **4**, 128.
18 D. B. Kirpotin, D. C. Drummond, Y. Shao, M. R. Shalaby, K. Hong, U. B. Nielsen, J. D. Marks, C. C. Benz and J. W. Park, *Cancer Res.*, 2006, **66**, 6732–6740.
19 D. W. Bartlett, H. Su, I. J. Hildebrandt, W. A. Weber and M. E. Davis, *Proc. Natl. Acad. Sci. U. S. A.*, 2007, **104**, 15549–15554.
20 O. C. Farokhzad, J. Cheng, B. A. Teply, I. Sherifi, S. Jon, P. W. Kantoff, J. P. Richie and R. Langer, *Proc. Natl. Acad. Sci. U. S. A.*, 2006, **103**, 6315–6320.
21 D. Peer, J. M. Karp, S. Hong, O. C. Farokhzad, R. Margalit and R. Langer, *Nat. Nanotechnol.*, 2007, **2**, 751–760.

22 N. Kamaly, Z. Xiao, P. M. Valencia, A. F. Radovic-Moreno and O. C. Farokhzad, *Chem. Soc. Rev.*, 2012, **41**, 2971–3010.
23 J. Shi, Z. Xiao, N. Kamaly and O. C. Farokhzad, *Acc. Chem. Res.*, 2011, **44**, 1123–1134.
24 Z. Cheng, A. Al Zaki, J. Z. Hui, V. R. Muzykantov and A. Tsourkas, *Science*, 2012, **338**, 903–910.
25 A. Koshkaryev, R. Sawant, M. Deshpande and V. Torchilin, *Adv. Drug Delivery Rev.*, 2013, **65**, 24–35.
26 N. Bertrand, J. Wu, X. Xu, N. Kamaly and O. C. Farokhzad, *Adv. Drug Delivery Rev.*, 2014, **66**, 2–25.
27 N. T. Tran, N. P. Truong, W. Gu, Z. Jia, M. A. Cooper and M. J. Monteiro, *Biomacromolecules*, 2013, **14**, 495–502.
28 E. K. Park, S. B. Lee and Y. M. Lee, *Biomaterials*, 2005, **26**, 1053–1061.
29 P. Chan, M. Kurisawa, J. E. Chung and Y.-Y. Yang, *Biomaterials*, 2007, **28**, 540–549.
30 M. O. Oyewumi, R. A. Yokel, M. Jay, T. Coakley and R. J. Mumper, *J. Controlled Release*, 2004, **95**, 613–626.
31 S. Mansouri, Y. Cuie, F. Winnik, Q. Shi, P. Lavigne, M. Benderdour, E. Beaumont and J. C. Fernandes, *Biomaterials*, 2006, **27**, 2060–2065.
32 S.-Q. Liu, N. Wiradharma, S.-J. Gao, Y. W. Tong and Y.-Y. Yang, *Biomaterials*, 2007, **28**, 1423–1433.
33 S. D. Weitman, R. H. Lark, L. R. Coney, D. W. Fort, V. Frasca, V. R. Zurawski and B. A. Kamen, *Cancer Res.*, 1992, **52**, 3396–3401.
34 D. Dubé, M. Francis, J.-C. Leroux and F. M. Winnik, *Bioconjugate Chem.*, 2002, **13**, 685–692.
35 S.-J. Yang, F.-H. Lin, K.-C. Tsai, M.-F. Wei, H.-M. Tsai, J.-M. Wong and M.-J. Shieh, *Bioconjugate Chem.*, 2010, **21**, 679–689.
36 A. B. Kunnumakkara, P. Anand and B. B. Aggarwal, *Cancer Lett.*, 2008, **269**, 199–225.
37 M. Akrami, M. Khoobi, M. Khalilvand-Sedagheh, I. Haririan, A. Bahador, M. A. Faramarzi, S. Rezaei, H. A. Javar, F. Salehi and S. K. Ardestani, *RSC Adv.*, 2015, **5**, 88096–88107.
38 E. I. Paramera, S. J. Konteles and V. T. Karathanos, *Food Chem.*, 2011, **125**, 913–922.
39 S. S. Bansal, M. Goel, F. Aqil, M. V. Vadhanam and R. C. Gupta, *Cancer Prev. Res.*, 2011, **4**, 1158–1171.
40 S. Jambhrunkar, Z. Qu, A. Popat, J. Yang, O. Noonan, L. Acauan, Y. Ahmad Nor, C. Yu and S. Karmakar, *Mol. Pharmaceutics*, 2014, **11**, 3642–3655.
41 R. Kotcherlakota, A. K. Barui, S. Prashar, M. Fajardo, D. Briones, A. Rodríguez-Diéguez, C. R. Patra and S. Gómez-Ruiz, *Biomater. Sci.*, 2016, **4**, 448–459.
42 S. Kim, S. Philippot, S. Fontanay, R. E. Duval, E. Lamouroux, N. Canilho and A. Pasc, *RSC Adv.*, 2015, **5**, 90550–90558.
43 H. Tang, J. Guo, Y. Sun, B. Chang, Q. Ren and W. Yang, *Int. J. Pharm.*, 2011, **421**, 388–396.
44 J. Zheng, X. Tian, Y. Sun, D. Lu and W. Yang, *Int. J. Pharm.*, 2013, **450**, 296–303.
45 B. Lindlar, A. Kogelbauer, P. J. Kooyman and R. Prins, *Microporous Mesoporous Mater.*, 2001, **44**, 89–94.
46 J. Zhang, M. Niemelä, J. Westermarck and J. M. Rosenholm, *Dalton Trans.*, 2014, **43**, 4115–4126.
47 L. Yuan, Q. Tang, D. Yang, J. Z. Zhang, F. Zhang and J. Hu, *J. Phys. Chem. C*, 2011, **115**, 9926–9932.
48 N. Lang and A. Tuel, *Chem. Mater.*, 2004, **16**, 1961–1966.
49 M. Gulfam and B. G. Chung, *Macromol. Res.*, 2014, **22**, 412–417.
50 B. Chertok, A. E. David and V. C. Yang, *Biomaterials*, 2010, **31**, 6317–6324.
51 A. Szegedi, M. Popova, I. Goshev, S. Klebert and J. Mihaly, *J. Solid State Chem.*, 2012, **194**, 257–263.
52 J. Shen, Q. He, Y. Gao, J. Shi and Y. Li, *Nanoscale*, 2011, **3**, 4314–4322.
53 M. M. Yallapu, S. F. Othman, E. T. Curtis, N. A. Bauer, N. Chauhan, D. Kumar, M. Jaggi and S. C. Chauhan, *Int. J. Nanomed.*, 2012, **7**, 1761–1779.
54 S. Alam, J. J. Panda and V. S. Chauhan, *Int. J. Nanomed.*, 2012, **7**, 4207–4222.
55 N. M. Khoram, B. Bigdeli, A. Nikoofar and B. Goliaei, *Int. J. Breast Cancer*, 2016, **19**, 18–25.
56 J. Li, L. Zheng, H. Cai, W. Sun, M. Shen, G. Zhang and X. Shi, *Biomaterials*, 2013, **34**, 8382–8392.
57 S. Mirsadeghi, R. Dinarvand, M. H. Ghahremani, M. R. Hormozi-Nezhad, Z. Mahmoudi, M. J. Hajipour, F. Atyabi, M. Ghavami and M. Mahmoudi, *Nanoscale*, 2015, **7**, 5004–5013.
58 M. Mahmoudi, I. Lynch, M. R. Ejtehadi, M. P. Monopoli, F. B. Bombelli and S. Laurent, *Chem. Rev.*, 2011, **111**, 5610–5637.
59 M. Mahmoudi, M. P. Monopoli, M. Rezaei, I. Lynch, F. Bertoli, J. J. McManus and K. A. Dawson, *ChemBioChem*, 2013, **14**, 568–572.
60 H. Jin, M. B. Ansari and S.-E. Park, *Chem. Commun.*, 2011, **47**, 7482–7484.
61 H. Song, C. Su, W. Cui, B. Zhu, L. Liu, Z. Chen and L. Zhao, *BioMed Res. Int.*, 2013, **2013**, 723158.
62 J. Ji, P. Zuo and Y.-L. Wang, *Nanoscale Res. Lett.*, 2015, **10**, 1–8.
63 J. Zhang, X. Li, J. M. Rosenholm and H.-c. Gu, *J. Colloid Interface Sci.*, 2011, **361**, 16–24.
64 S. Brunauer, P. H. Emmett and E. Teller, *J. Am. Chem. Soc.*, 1938, **60**, 309–319.
65 E. P. Barrett, L. G. Joyner and P. P. Halenda, *J. Am. Chem. Soc.*, 1951, **73**, 373–380.
66 L. Jia, J. Shen, Z. Li, D. Zhang, Q. Zhang, C. Duan, G. Liu, D. Zheng, Y. Liu and X. Tian, *Int. J. Pharm.*, 2012, **439**, 81–91.
67 Y. Xiao, H. Hong, A. Javadi, J. W. Engle, W. Xu, Y. Yang, Y. Zhang, T. E. Barnhart, W. Cai and S. Gong, *Biomaterials*, 2012, **33**, 3071–3082.
68 A. Pourjavadi and Z. M. Tehrani, *Int. J. Polym. Mater. Polym. Biomater.*, 2014, **63**, 692–697.
69 V. Dodane, M. A. Khan and J. R. Merwin, *Int. J. Pharm.*, 1999, **182**, 21–32.
70 M. Torkpur-Biglarianzadeh and M. Salami-Kalajahi, *RSC Adv.*, 2015, **5**, 29653–29662.
71 P. Costa and J. M. S. Lobo, *Eur. J. Pharm. Sci.*, 2001, **13**, 123–133.
72 A. R. Khare and N. A. Peppas, *Biomaterials*, 1995, **16**, 559–567.

73 Y. Gao, Y. Li, Y. Li, L. Yuan, Y. Zhou, J. Li, L. Zhao, C. Zhang, X. Li and Y. Liu, *Nanoscale*, 2015, **7**, 597–612.
74 A. Kunwar, A. Barik, B. Mishra, K. Rathinasamy, R. Pandey and K. Priyadarsini, *Biochim. Biophys. Acta, Gen. Subj.*, 2008, **1780**, 673–679.
75 S. Honary and F. Zahir, *Trop. J. Pharm. Res.*, 2013, **12**, 255–264.
76 D. Feng, Y. Song, W. Shi, X. Li and H. Ma, *Anal. Chem.*, 2013, **85**, 6530–6535.
77 L. Jiang, Z.-m. Gao, L. Ye, A.-y. Zhang and Z.-g. Feng, *Biomater. Sci.*, 2013, **1**, 1282–1291.
78 S. Jambhrunkar, S. Karmakar, A. Popat, M. Yu and C. Yu, *RSC Adv.*, 2014, **4**, 709–712.
79 C. C. Fleischer and C. K. Payne, *Acc. Chem. Res.*, 2014, **47**, 2651–2659.